Temperature Dependence of the Solubility of Carbon Dioxide in Imidazolium-Based Ionic Liquids

Daniela Kerlé,[†] Ralf Ludwig,*[,†,‡] Alfons Geiger,[§] and Dietmar Paschek*[,⊥]

Institut für Chemie, Abteilung Physikalische Chemie, Universität Rostock, Dr.-Lorenz-Weg 1, D-18051 Rostock, Germany, Leibniz-Institut für Katalyse an der Universität Rostock, A.-Einstein-Strasse 29a, D-18059 Rostock, Germany, Fakultät Chemie, Physikalische Chemie, TU Dortmund, Otto-Hahn-Strasse 6, D-44221 Dortmund, Germany, and Department of Physics, Applied Physics & Astronomy, Rensselaer Polytechnic Institute, 110 Eighth Street, Troy, New York 12180

Received: June 12, 2009; Revised Manuscript Received: July 31, 2009

The solubility of carbon dioxide in ionic liquids of type 1-alkyl-3-methylimidazolium bis(trifluoromethylsulfonyl)imide ($[C_n\text{mim}][NTf_2]$) with varying chain length $n = 2, 4, 6, 8$ is computed from molecular dynamics simulations. By applying both Bennett's overlapping distribution method and Widom's particle insertion technique, we determine solvation free energies that are in excellent agreement with available experimental solubility data over a large temperature range from 300 to 500 K. We find that the computed solvation free energy of carbon dioxide is remarkably insensitive to the alkane chain length, emphasizing the importance of solvent models with accurate volumetric properties. The simulations suggest that the "anomalous" temperature dependence of the CO_2 solvation at infinite dilution is characterized by counter-compensating negative entropies and enthalpies of solvation. By systematically varying the interaction strength of CO_2 with the solvent, we show that the negative solvation entropy of CO_2 is not caused by solvation cavities, but enforced by Coulomb and van der Waals interactions. We observe that solvation free energies and enthalpies obtained for models with different solute−solvent interaction strengths are subject to a linear correlation, similar to an expression that has been suggested for gases in polymers. Despite the apparent chain length insensitivity of the solvation free energy, significant changes in the solvation shell of a CO_2 molecule are observed. The chain length insensitivity is found to be a consequence of two counter-compensating effects: the increasing free energy of cavity formation is balanced by a favorable interaction of CO_2 with the alkyl chain of the imidazolium cation.

1. Introduction

Organic salts with melting points below 100 C are now commonly referred to as ionic liquids (ILs). These liquids represent a relatively new class of nonmolecular materials with unique properties.[1−3] The interest in these materials is stimulated by a wide range of potential applications: for example, as solvents for reactions and material processing, as extraction media, or as working fluids for mechanical devices. For many of those applications, knowledge of the physical properties of the ILs is often an essential necessity. Prominent features of ILs are their famously low volatility, low viscosity, and high ionic conductivity, as well as good thermal and electrochemical stability. The variability of the ions often allows the properties of interest to be imparted so that ILs have been described as "designer solvents". The ionic nature of ILs has important consequences for the structure of the liquid on the nanoscopic level.[4,5] Spectroscopic evidence suggests the presence and importance of the formation of intermolecular cation/anion hydrogen bonds.[6] Favorable and specific anion/cation interactions seem to induce the formation of a persistent anion/cation network, which has been shown to be quite tolerable to adding both polar and apolar particles.[7]

Recently, systematic measurements of the infinite dilution properties for a number of gases, including methane, carbon dioxide, and the noble gases have been reported.[8−22] In particular, the phase behavior of CO_2 with ILs might be important for the development of potential carbon sequestration applications.[23] Brennecke et al. showed that CO_2 was soluble in certain ILs and that it could be used to extract organic solutes.[24−26] They also demonstrated that CO_2 could increase the solubility of gases that are not very soluble on their own.[27] In addition, it was found that the bis(trifluoromethylsulfonyl)imide ($[NTf_2]^-$) anion has the greatest affinity for CO_2.

Molecular dynamics (MD) and Monte Carlo (MC) simulations provide a powerful means for gaining fundamental understanding of the mechanism for the high solubility of CO_2 in imidazolium-based ILs. The solubilities of CO_2 in the ionic liquid 1-*n*-hexyl-3-methylimidazolium bis(trifluoromethylsulfonyl)imide ($[C_6\text{mim}][NTf_2]$) came out quite well because most of the "static" properties simulated with available classical force fields.[4,22,28−31] Because many force fields were not found to describe transport properties such as diffusion coefficients and viscosities satisfactorily, we have recently suggested modifying the Lennard-Jones interactions in the nonpolarizable all-atom force field of Lopes et al.[32] for imidazolium-based ILs of the type $[C_n\text{mim}][NTf_2]$.[33] We have shown that a wealth of thermodynamical and dynamical properties of the pure IL could be obtained in excellent agreement with experimental data.[33,34] The modified force field was also capable of describing the solvation behavior of small apolar particles.[35] We could demonstrate that the solvation is characterized by an enthalpy/

* To whom correspondence should be addressed. E-mail: (R.L.) ralf.ludwig@uni-rostock.de, (D.P.) paschd3@rpi.edu.
† Institut für Chemie, Abteilung Physikalische Chemie, Universität Rostock.
‡ Leibniz-Institut für Katalyse an der Universität Rostock.
§ TU Dortmund.
⊥ Rensselaer Polytechnic Institute.

10.1021/jp9055285 CCC: $40.75
Published on Web 09/01/2009

entropy compensation effect, not unlike the hydrophobic hydration of small apolar particles in liquid water.[36−39] Moreover, an entropy-driven "solvophobic interaction" of apolar particles was also observed,[35] suggesting that specific solvent-mediated interactions could be an important feature of ILs.

Substantial efforts to study the solvation behavior of solutes in ionic liquids by simulation methods were reported earlier. Lynden-Bell and co-workers investigated the infinite dilution behavior of a series of small and larger cyclic molecules in dimethyl imidazolium chloride using thermodynamic integration.[40,41] The same method was used by Deschamps et al. for investigating solubility trends of gases in ILs.[42] Maginn et al. have used particle insertion methods[43] as well as expanded ensemble techniques[44] to study the solubility of a range of different gases in 1-*n*-butyl-3-methylimidazolium hexafluorophosphate ([C_4mim][PF_6]). In particular, they focused on understanding the origin of the high solubility of CO_2 in ILs using molecular dynamics simulations.[9] Maurer and co-workers estimated the solubility of oxygen, carbon dioxide, carbon monoxide, and hydrogen in the ionic liquid 1-*n*-butyl-3-methylimidazolium hexafluorophosphate.[45−47] Quite recently, Maginn et al. developed a Monte Carlo sampling procedure that is particularly well-suited for computing gas solubility in dense media, such as ionic liquids.[43,44] Using their continuous fractional component Monte Carlo method (CFC MC), they reported solubilities of CO_2 and H_2O in the ionic liquid 1-*n*-hexyl-3-methylimidazolium bis(trifluoromethylsulfonyl)imide ([C_6mim][NTf_2]) at finite carbon dioxide concentrations.[48]

Here, we focus on the infinite dilution properties of carbon dioxide. We apply Bennett's overlapping distribution method as well as Widom's particle insertion technique for calculating solvation free energies and solubilities of CO_2 in imidazolium-based ionic liquids of the type [$C_n$mim][NTf_2] with $n = 2, 4, 6, 8$. The calculated Henry constants are compared with experimental data. The temperature behavior of the solubility as well as its dependence on the alkyl chain length in the imidazolium cations is determined. Particular attention is paid to the interaction strength of the carbon dioxide molecule with its environment. Ultimately, we separate the "cavity contribution" of the solvation free energy as determined from a hypothetical purely repulsive CO_2 molecule interacting with its environment due to a Weeks−Chandler−Andersen (WCA) potential.[49] Implications of the observed behavior for the corresponding entropic and enthalpic contributions are discussed.

2. Experimental Section

2.1. Molecular Dynamics Simulations. We perform constant pressure (NPT) MD simulations of imidazolium-based ILs of the type [C_2mim][NTf_2] for different chain lengths $n = 2, 4, 6, 8$ at a pressure of 1 bar, covering a broad temperature range between 300 and 500 K. All simulated systems are composed of 343 ion pairs, applying our recently proposed modifications[33] to the Lopes et al. force field.[32] In addition, all systems also contain one single molecule of carbon dioxide, employing the EPM2 model of Harris and Yung.[50] Deviating from the original paper of Harris and Yung, the CO_2 molecule is treated as a rigid linear rotator[50] by shifting the forces acting on the interaction sites to a diatomic molecule with similar mass and moment of inertia.[51] Independent simulations of pure supercritical and liquid carbon dioxide composed of rigid EPM2 molecules reveal excellent agreement with available thermodynamic and kinetic data.[52,53] A minor modification from the simulation setup used in previous studies[33,34] is that all bond lengths were kept fixed.

TABLE 1: Mass Densities As a Function of Temperature and Chain Length, C_n, for the Studied Series of Ionic Liquids[a]

	ρ/g cm^{-3}			
T/K	[C_2mim]	[C_4mim]	[C_6mim]	[C_8mim]
	MD Simulation			
300	1.499	1.427	1.366	1.331
350	1.436	1.366	1.308	1.278
400	1.374	1.308	1.252	1.225
450	1.317	1.253	1.199	1.173
500	1.261	1.200	1.147	1.123
	Experimental Data			
300	1.513	1.434	1.368	1.315
350	1.463	1.387	1.323	1.271
400	1.415	1.341	1.280	1.229

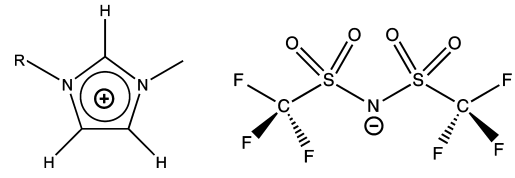

[a] MD simulation: Each simulation contains 343 ion pairs plus one CO_2 molecule. Data were obtained at at a pressure of 1 bar. The statistical uncertainty of the shown data has been estimated to be below ± 0.001 g cm^{-3} according to a block-averaging procedure.[63] Experimental data: Densities were calculated from fitted data reported by Tariq et al.[62]

All simulations reported here were performed with the Gromacs 3.2 simulation program.[54] The preparation of topology files as well as the data analysis was performed with the most recent version of the MOSCITO suite of programs.[55] Gromacs topology and restart files are availabe on request. Production runs of 10 ns length were employed for every temperature, starting from previously equilibrated configurations. The Nosé−Hoover thermostat[56,57] and the Parrinello−Rahman barostat[58,59] with coupling times $\tau_T = 1.0$ ps and $\tau_p = 2.0$ ps were used to control constant temperature and pressure (1 bar) conditions. The electrostatic interactions were treated by particle mesh Ewald summation.[60] A real space cutoff of 1.2 nm was employed, and a mesh spacing of approximately 0.12 nm (fourth-order interpolation) has been used to determine the reciprocal lattice contribution. The Ewald convergence parameter was set to a relative accuracy of the Ewald sum of 10^{-5}. Lennard-Jones cutoff corrections for energy and pressure were considered. A 2 fs time step was used, and every 25 steps, a configuration was saved. Distance constraints were solved by the SHAKE procedure.[61] Despite minor modifications compared to ref 33 (larger system size, all bond-length-constrained), no substantial deviations from the dynamic and thermodynamic properties reported previously are denoted. The densities for all simulated systems and temperatures are summarized in Table 1 and are found to be almost quantitatively consistent with a recent systematic study of densities reported by Tariq et al.[62] A more detailed discussion of the thermodynamic and dynamical properties of these ILs can be found in ref 33.

2.2. Infinite Dilution Properties. The solubility of a gaseous solute is conveniently described by the Ostwald coefficient $L^{l/g} = \rho_B^l/\rho_B^g$, where ρ_B^l and ρ_B^g are the number densities of the solute in the liquid and the gas phase, respectively, when both phases are in equilibrium. Here, A denotes the solvent and B indicates the solute. Equilibrium between both phases leads to a new expression for $L^{l/g}$, namely,

$$L^{l/g} = \exp[-\beta(\mu^{l}_{ex,B} - \mu^{g}_{ex,B})] \quad (1)$$

where $\beta = 1/kT$ and $\mu^{l}_{ex,B}$ and $\mu^{g}_{ex,B}$ denote the excess chemical potentials of the solute in the liquid and the gas phase, respectively. When the gas phase has a sufficiently low density (which is an excellent approximation for the case of ILs) then $\mu^{g}_{ex,B} \approx 0$; hence, $L^{l/g}$ becomes identical to the solubility parameter $\gamma^{l}_{B} = \exp[-\beta\mu^{l}_{ex,B}]$.

As an alternative to the Ostwald coefficient, the solubility of gases is expressed in terms of the inverse Henry's constant k_H^{-1}. The relationship between Henry's constant and the excess chemical potential in the liquid phase is given by[64]

$$k_H^{-1} = \exp[-\beta\mu^{l}_{ex,gas}]/\rho^{l}_{IL}RT \quad (2)$$

where ρ^{l}_{IL} represents the number density of ion pairs in the IL solvent.

According to Widom's potential distribution theorem,[65,66] the excess chemical potential, μ_{ex}, can be computed as a volume-weighted ensemble average.

$$\mu_{ex} = -kT \ln\langle V \exp(-\beta\Phi)\rangle/\langle V\rangle \quad (3)$$

Here, $\beta = 1/kT$, V is the volume of the simulation box, and Φ is the energy of a gas molecule inserted at a random position with a random orientation. The parentheses indicate isothermal−isobaric averaging over many configurations, as well as averaging over many insertions.

As control, we also determine the excess chemical potential from energy histograms[67,68] computed for the energy change, ΔU, associated with the insertion ($p_0(\Delta U)$) and removal ($p_1(\Delta U)$) of a CO_2 molecule from the constant pressure (NPT) simulation. The two distribution functions are related according to

$$p_1(\Delta U) = \frac{Q(N,P,T)}{Q(N+1,P,T)}\frac{\langle V\rangle}{\Lambda^3} \times \exp(-\beta\Delta U)\, p_0(\Delta U) \quad (4)$$

Using the definition of the *ideal* and *excess* part of the chemical potential μ referring to the ideal gas state with the same average number density,[69] a relation between the two distribution functions and the excess chemical potential is obtained, which is analogous to the expression for the canonical ensemble[69]

$$\ln p_1(\Delta U) - \ln p_0(\Delta U) = \beta\mu_{ex} - \beta\Delta U \quad (5)$$

The only difference is the necessity of *volume-weighting* in the calculation of the $p_0(\Delta U)$ distribution function.[70] For reasons of convenience, we define functions f_0 and f_1 according to

$$f_0(\Delta U) = \beta^{-1}\ln p_0(\Delta U) - \frac{\Delta U}{2} \quad \text{and}$$

$$f_1(\Delta U) = \beta^{-1}\ln p_1(\Delta U) + \frac{\Delta U}{2}$$

such that

$$\mu_{ex} = f_1(\Delta U) - f_0(\Delta U) \quad (6)$$

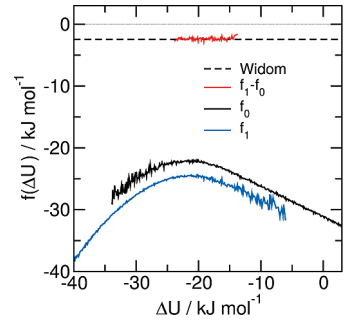

Figure 1. Excess chemical potential μ_{ex} of CO_2 dissolved in [C_6mim][NTf_2] at 300 K and 1 bar according to the overlapping distribution method. Shown are the energy histograms $f_1(\Delta U)$ and $f_0(\Delta U)$ as well as their difference, $\mu_{ex} = f_1 - f_0$. The dashed line represents the value according to Widom's particle insertion technique. The $f_1 - f_0$ data shown here have a weight of at least 20% of the maximum statistical weight, as computed from the p_0 and p_1 functions.

TABLE 2: Excess Chemical Potentials μ_{ex} (given in kJ mol^{-1}) of Carbon Dioxide in Imidazolium-Based Ionic Liquids [$C_n$mim][NTf_2] with n = 2, 4, 6, 8 As a Function of Temperature[a]

	$\mu_{ex}(CO_2)$/kJ mol^{-1}			
T/K	[C_2mim]	[C_4mim]	[C_6mim]	[C_8mim]
300	−2.54 ± 0.21	−2.77 ± 0.24	−2.37 ± 0.22	−2.86 ± 0.23
350	−0.59 ± 0.21	−0.77 ± 0.18	−0.89 ± 0.17	−0.99 ± 0.17
400	0.60 ± 0.19	0.51 ± 0.18	0.48 ± 0.18	0.46 ± 0.18
450	1.86 ± 0.19	1.60 ± 0.20	1.57 ± 0.19	1.52 ± 0.19
500	2.79 ± 0.19	2.64 ± 0.20	2.43 ± 0.19	2.63 ± 0.19

[a] The data shown were computed from weighted averages of the free energy differences according to the energy histograms of particle insertion and removal.

All computed energies are based on the minimum image and include a reaction field correction similar to Roberts and Schnitker.[71] Cut-off corrections for the dispersion interactions are included.[72] Note that we have computed both f_0 and f_1 functions from the same set of simulations, containing a single carbon dioxide molecule. Considering the large size of the system, the perturbation of f_0 caused by the presence of a single carbon dioxide molecule is deemed negligible.

A total of 2×10^5 configurations were analyzed for each ionic liquid and for every temperature. Each configuration was sampled by 10^3 random insertions to determine the f_0 functions. The energies computed for those insertions has also been used to determine "Widom estimates" for the excess chemical potentials. Figure 1 depicts the f_0 and f_1 distribution functions obtained for carbon dioxide dissolved in [C_6mim][NTf_2] at 300 K. Figure 1 indicates a large region of overlap, providing a reliable basis to estimate the solvation free energies, $\mu_{ex} = f_1(\Delta U) - f_0(\Delta U)$, given in Table 2. The reported data are obtained as weighted averages,[69] computing the weights from the p_0 and p_1 distributions. Similarly well overlapping distribution functions were obtained for all simulations discussed in this paper. We would like to point out that the values computed from particle insertions are found to lie within the statistical uncertainty of the data given in Table 2. Initially, this observation came to us quite as a surprise, since it has been recently argued that solubilities obtained from insertion techniques are prone to systematic errors.[22] However, the form of the f_0 function in Figure 1 points to an explanation of why the $f_1 - f_0$ data and the Widom data match. The agreement of the data shown is plausible, since a well-represented left shoulder of the f_0

TABLE 3: Calculated Henry Constants for CO_2 in Ionic Liquids of Type [$C_n$mim][NTf_2] at 1 Bar for the Case of Infinite Dilution According to $k_H = \exp[\beta\mu^l_{ex,gas}] \times \rho^l_{IL}RT$[64] Obtained from the MD Simulations

	$k_H(CO_2)$/bar			
T/K	[C_2mim]	[C_4mim]	[C_6mim]	[C_8mim]
300	34 ± 3	28 ± 3	29 ± 3	22 ± 3
350	87 ± 6	73 ± 5	63 ± 4	56 ± 6
400	140 ± 8	121 ± 6	107 ± 6	98 ± 9
450	207 ± 10	171 ± 9	152 ± 8	139 ± 11
500	262 ± 12	224 ± 11	191 ± 9	185 ± 13

distribution suggests ample sampling of low-energy configurations by CO_2 insertions. Note that the choice of the sampling rate is a critcal parameter for successfully computing the chemical potentials via Widom's insertion technique. By systematically reducing the sampling rate, we observe a systematic deviation of the "Widom estimate" from the chemical potential data reported in Table 2, if sampling rates of about 2 orders of magnitude lower than the rates reported here are used.

3. Results and Discussion

We have computed the solvation free energy, μ_{ex}, of CO_2 at infinite dilution from MD simulations for the four ionic liquids [$C_n$mim][NTf_2] with $n = 2, 4, 6, 8$ employing the overlapping distribution method as discussed in the previous section. All solvation free energy data are given in Table 2. The corresponding Henry constants are reported in Table 3. In Figure 2, the simulated CO_2 solubilities (given as inverse Henry's constant) are compared to recently published experimental data by Cadena et al.,[9] Camper et al.,[10−12] Finotello et al.,[13] and Jacquemin et al.[21] for [C_2mim][NTf_2]; Baltus et al.,[14] Lee et al.,[15] Anthony et al.,[17] Kumelan et al.,[18] Finotello et al.,[13] Gomes,[19] and Muldoon et al.[20] for [C_6mim][NTf_2]; and Baltus et al.[14] for [C_8mim][NTf_2], respectively. For [C_6mim][NTf_2], we have also included the data of Shi and Maginn,[22] which were obtained from computer simulations using their continuous fractional component CFC MC technique. We would like to emphasize that without modifying the carbon dioxide−IL interaction, the computed solubility data are found to be in excellent agreement with most of the available experimental data. Considering the scatter of the experimental data from various sources as well as the statistical uncertainty of our simulated data, only the data of Baltus et al.[14] for [C_4mim][NTf_2] and [C_8mim][NTf_2] seem to be deviating significantly. In both cases, Baltus et al. report markedly lower solubilities. Unfortunately, Baltus et al.[14] are the only available source for [C_8mim][NTf_2]. The overall good agreement in general is consequently also found for the temperature dependence of the solubility data. The solubility data for [C_6mim][NTf_2] are available over a large temperature range and have been measured by many groups. This is fortunately due to the fact that [C_6mim][NTf_2] has been selected as a reference ionic liquid for an IUPAC experimental validation project.[74,75] The computed solubilities between 300 and 450 K are found to be compatible with the high temperature inverse Henry constants reported by Kumelan et al.[18] The solubilities reported by Shi and Maginn of CO_2 in [C_6mim][NTf_2] from CFC MC simulation also agree very favorably with the experimental data, although for the highest temperatures, their data seem to deviate slightly more strongly from Kumelan's data[18] than do ours. However, it might require more experimental data and simulations for a fair judgment about the quality of the different IL models employed. The overall favorable agreement with experimental data might be considered as a further justification for the modifications that were applied to the Lopez et al. force field. In addition, our calculations demonstrate that both the overlapping distribution method and the Widom particle insertion technique are suitable to determine CO_2 solubilities in ionic liquids from molecular dynamics simulation data, if carried out carefully.

The chain length dependence of the solvation free energy is shown in Figure 3a and Table 2. The data show surprisingly little variation for ILs with different chain lengths. There is only a slight tendency toward lower solvation free energies for longer chains, when comparing [C_2mim][NTf_2] and [C_8mim][NTf_2]. In addition, these changes are found to be temperature-insensitive. The increase in the solubility of CO_2, which has been observed by Fintonello et al.[13] and which is evident from the inverse Henry constants shown in Figure 3b, is hence almost

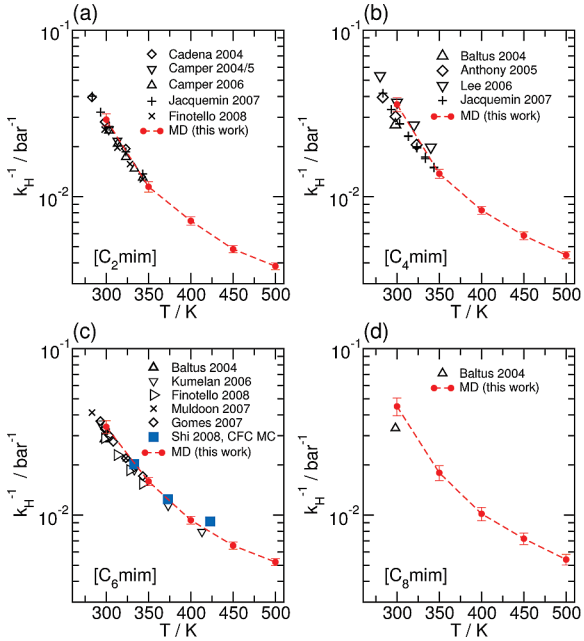

Figure 2. Solubilities $k_H^{-1} = \exp[-\beta\mu^l_{ex,gas}]/\rho^l_{IL}RT$[64] of CO_2 in (a) [C_2mim][NTf_2], (b) [C_4mim][NTf_2], (c) [C_6mim][NTf_2], and (d) [C_8mim][NTf_2] at 1 bar. The red circles represent data obtained from the MD simulations (see Table 3). The experimental data are according to Cadena et al.,[9] Camper et al.,[10−12] Finotello et al.,[13] Baltus et al.,[14] Lee et al.,[15] Anthony et al.,[17] Kumelan et al.,[18] Gomes,[19] Muldoon et al.,[20] and Jacquemin et al.[21] The blue squares shown in panel c are according to Shi and Maginn,[22] obtained from CFC MC simulations. The statistical uncertainty of the individual experimental data points shown is roughly approximated by the chosen symbol sizes.

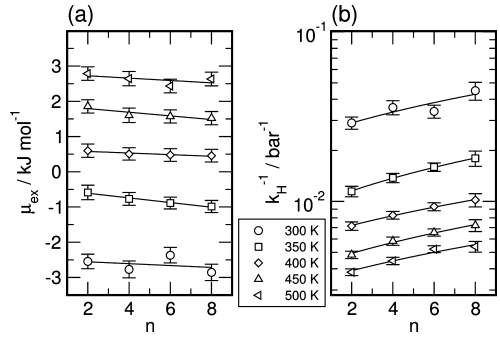

Figure 3. (a) Excess chemical potential, $\mu^l_{ex,gas}$, and (b) solubility, $k_H^{-1} = \exp[-\beta\mu^l_{ex,gas}]/\rho^l_{IL}RT$[64] of CO_2 in [$C_n$mim][NTf_2] with $n = 2, 4, 6, 8$ for all simulated temperatures at 1 bar. The lines represent linear fits and are intended as a guide to the eye.

solely caused by the increasing molar volume of the IL with increasing chain length. Consequently, for a reliable prediction of solubility data, an accurate representation of the volumetric properties of the solvent is of considerable importance.

Having computed the temperature-dependent solvation free energy for inifinite dilution, we can also comment on the behavior of the first and second derivatives of free energy with respect to temperature. The solvation entropies, enthalpies, and heat capacities are obtained from fits of the data to a second-order expansion of the solvation free energy around reference state ($T^0 = 298$ K at $P^0 = 1$ bar) according to

$$\mu_{ex}(T) = \mu^0_{ex} - s^0_{ex}(T - T^0) - c_{P,ex}[T(\ln T/T^0 - 1) + T^0] \quad (7)$$

Here, μ^0_{ex} and s^0_{ex} represent the solvation free energy and solvation entropy at the reference state, respectively. According to the second order expansion, the solvation heat capacity $c_{P,ex}$ is assumed to be constant over the considered temperature range. The fitted values are provided in Table 5. All temperature-dependent enthalpies and entropies shown in related Figures have been computed from those fits. First of all, we point out the fact that CO_2 exhibits an "anomalous" solvation behavior, showing a decreasing solubility with increasing temperature. Although this behavior is slightly enforced by the decreasing solute density, it is predominantly due to CO_2's negative solvation entropy (see Table 5). Thermodynamically caused anomalous solvation has been reported for nonpolar molecule dissolved network-forming liquids, such as water, where the term "hydrophobic hydration" has been established,[36,37] but it has also been reported for the solubility of gases in polymers[76,77] as well as for several molecular liquids.[78] In the case of water, such a behavior has been explained as due to the molecular reorganization of the water molecules in the hydration shell of an apolar molecule, since water aims to maintain an intact hydrogen bond network.[37] In the case of nonpolar polymers, the solute affects the configurational entropy of the polymer chains, constrained by intrapolymer bonds, and has been described in the framework of lattice fluid[79] and lattice hole theory.[73,80] Interestingly, ionic liquids are positioned between those two extremes. On one hand, ILs share similarities with water because they are molecular fluids and exhibit a substantial degree of intermolecular order. On the other hand, CO_2 is considerably smaller than the constituents of the ionic liquids, whereas hydrophobic solutes are at least of the size of a water molecule. An apparent thermodynamic similarity with the hydrophobic hydration is that relatively small absolute solvation free energies are a consequence of large counter-compensating negative enthalpic and entropic contributions. In addition, a positive heat capacity of solvation has been related to the increasingly disintegrating hydrogen bond network at elevated temperatures. As shown in Table 5, the Ils exhibit quite similar features. At standard conditions, the solvation enthalpies are about 5−6 times larger than the solvation free energies, and a positive heat capacity of about ≈ 40 JK^{-1} mol^{-1} is found. For the case of hydrophobic hydration, this effect has been shown to be intimately related to pure solvent properties, caused by the presence of preexisting cavities in the water structure which are structurally very similar to a hydrophobic hydration shell. As a consequence, even a fully repulsive, hard-core, small-size solute has been shown to exhibit a negative solvation entropy and a positive solvation heat capacity.[81] To investigate whether similar thermodynamical principles are at play in ionic liquids,

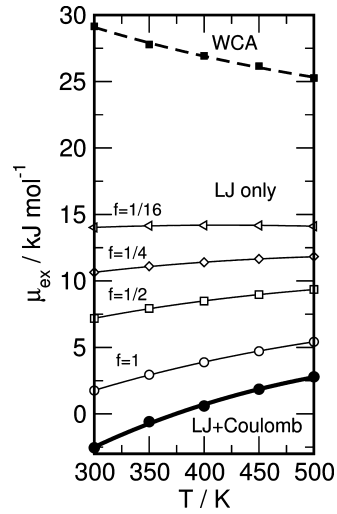

Figure 4. Temperature dependence of the excess chemical potential, μ_{ex}, of CO_2 dissolved in [C_2mim][NTf_2]. Solid circles: complete, unscaled interaction (Lennard-Jones plus Coulomb) of CO_2 with the IL solvent. Open symbols: only Lennard-Jones interactions are considered, and scaled by a factor f with $\varepsilon_{ij} = (f\varepsilon_{ii}\varepsilon_{jj})^{1/2}$ to vary the interaction strength. Solid squares: excess chemical potentials obtained for the purely repulsive WCA-CO_2. The lines represent fits to the second-order expansion of the solvation free energy with respect to temperature given in eq 7.

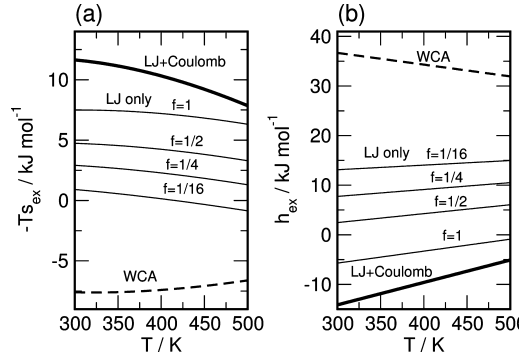

Figure 5. Enthalpic and entropic contributions to the solvation free energy $\mu_{ex} = h_{ex} - Ts_{ex}$ for CO_2 dissolved in [C_2mim][NTf_2] obtained as temperature derivatives $h_{ex} = -T^2[\partial(\mu_{ex}/T)/\partial T]_P$, and $s_{ex} = -[\partial\mu_{ex}/\partial T]_P$ of fits to the second order expansion of the solvation free energy given by eq 7. Exactly the same potential model variants are shown as used in Figure 4.

we have determined cavity contributions for the solvation of CO_2 dissolved in the ILs by systematically modifying the solute−solvent interaction. Therefore, we have calculated solvation free energies for CO_2 with zero partial charges and increasingly weakened solute−solvent Lennard-Jones interactions. Here, the Lennard-Jones ε_{ij} were scaled by a factor f with $\varepsilon_{ij} = (f\varepsilon_{ii}\varepsilon_{jj})^{1/2}$, with a large variation in interaction strength, as demonstrated in Figures 4 and 5. Ultimately, we also consider a purely repulsive Weeks−Chandler−Andersen type potential[49] for CO_2 referred to as WCA-CO_2, with $V_{ij}(r) = V_{LJ,ij}(r) + \varepsilon_{ij}$ for $r \le r_{LJ,min}$, and $V_{ij}(r) = 0$, otherwise. Here $r_{LJ,min} = 2^{1/6}\sigma_{ij}$ corresponds to the distance of the Lennard-Jones potential energy minimum for each of the possible pairwise solute−solvent Lennard-Jones interactions. To compute the solvation free energies for those models, we have applied two strategies: First, we have computed data employing the Widom particle insertion technique, applying exactly the same conditions as before for CO_2. Alternatively, we also have computed the free energy change for transforming a dissolved carbon dioxide molecule into a modified potential variant by free energy perturbation[82] according to

$$\Delta G = -kT \ln \langle \exp(-\beta \Delta U) \rangle_0 \quad (8)$$

where $\Delta U = U_1 - U_0$ represents the energy difference of replacing the conventional solute−solvent interaction, U_0, with a modified potential interaction model U_1, and $\langle \cdots \rangle_0$ indicates isobaric−isothermal averaging over state "0". In all cases reported here, we have obtained consistent solvation free energies using both methods. The largest free energy differences, of course, were observed for transforming a carbon dioxide molecule into a completely repulsive WCA model. The data calculated by both methods for $[C_2mim][NTf_2]$ are summarized in Table 4. The agreement between those two complementary approaches suggests that the obtained solvation free energies and their temperature derivatives can be considered reliable. The temperature-dependent solvation free energies shown in Figure 4 indicate that weakening the solute−solvent interaction is accompanied by a qualitative change in temperature dependence, finally leading to a change in sign of the associated solvation entropy for the purely repulsive model, as shown in Figure 5, and indicated in Table 5. Hence, the creation of a cavity of the size of a CO_2 molecule is accompanied by a large positive entropy, presumably creating a certain amount of disorder in the ionic liquid solvent. The large positive solvation free energy of about 30 kJ mol^{-1} also suggests that cavities of the size of a carbon dioxide molecule are vary rare. A "void-filling" adsorption mechanism, as suggested by Blanchard et al.,[25] does not seem to be very likely. The data calculated for CO_2 with varying interaction strength, shown in Figures 4 and 5, indicate that both the enthalpic and entropic contributions change concertedly. A similar behavior has been observed experimentally when comparing similar enthalpic and entropic contributions of various gases with one another.[17] The large positive solvation enthalpies observed for a weakly interacting solute are connected with positive solvation entropies, whereas the negative solvation enthalpy observed for the (unmodified) CO_2 molecule is related to a negative solvation entropy. This might be due to introducing a certain degree of order into the solvent. An alternative explanation might be that favorable interactions are restricting the configurational space of the solute molecule. In the latter scenario, the increasingly attractive interaction would "funnel" the molecule toward more attractive "binding sites". Simha and co-workers showed that the solubility of different gases in the same polymer, plotted on a logarithmic scale, are linearly related to their solvation enthalpy.[73] In a similar fashion, we present here the solvation free energy of the different carbon dioxide variants as a function of their solvation enthalpy. In Figure 6, we show data for $[C_2mim][NTf_2]$ obtained under standard conditions. Quite remarkably, a linear relation is obtained with a slope of 0.63, suggesting a similarly linear, but nontrivial, enthalpy−entropy relation, which possibly depends on the solvent. Given the relatively small changes found for the solvation free energies for the different IL solvents, however, those changes might not be very dramatic. In addition, comparing the data for CO_2, WCA-CO_2, and CO_2 ($f = 1$), shown in Figures 6 and 5, we can conclude that the majority of the attractive interaction of CO_2 with the ILs is due to the van der Waals interactions. The Coulomb interaction contributes only about 10% to the total solvation enthalpy. This observation supports arguments recently raised by Scovazzo et al.,[83] who were suggesting that the consistency of their data with the regular solution theory indicates a dominance of "short range" molecular interactions in ILs.

In the previous section, we pointed out the fact that the solvation free energies of CO_2 computed for the different ILs vary only weakly with alkane chain lengths. However, a substantially more significant change is observed if the fully repulsive WCA-CO_2 is considered (see Figure 7 and data in Table 5). This seems to indicate that the apparent chain length insensitivity of CO_2 is not due to the absence of any significant changes in the environment of a CO_2 molecule per se, but is

TABLE 4: Excess Chemical Potential of the Purely Repulsive WCA − CO_2 Dissolved in $[C_2mim][NTf_2]$ at 1 bar[a]

	ΔG/kJ mol^{-1}		
T/K	$\Delta G(CO_2 \rightarrow$ WCA-$CO_2)$	$\mu_{ex}(CO_2) + \Delta G(CO_2 \rightarrow$ WCA-$CO_2)$	μ_{ex}(WCA-CO_2)
300	31.6 ± 0.7	29.0 ± 0.8	28.4 ± 0.4
350	28.6 ± 0.4	28.0 ± 0.5	27.5 ± 0.2
400	26.4 ± 0.4	27.0 ± 0.4	26.7 ± 0.1
450	24.5 ± 0.2	26.3 ± 0.3	26.0 ± 0.1
500	22.6 ± 0.1	25.4 ± 0.2	25.3 ± 0.1

[a] $\Delta G(CO_2 \rightarrow$ WCA-$CO_2)$ is calculated by free energy perturbation of the original CO_2 molecule. The $\mu_{ex}(CO_2)$ data used here were taken from Table 2. The μ_{ex}(WCA-CO_2) data shown in the right column has been determined using the Widom particle insertion technique.

TABLE 5: Thermodynamic Parameters Describing the Temperature Dependence of the Solvation Free Energy $\mu_{ex}(T)$ of CO_2 and the Purely Repulsive Potential Model Variant WCA-CO_2[a]

	CO_2				WCA-CO_2	
	$[C_2mim]$	$[C_4mim]$	$[C_6mim]$	$[C_8mim]$	$[C_2mim]$	$[C_8mim]$
μ^0_{ex}/kJ mol^{-1}	−2.57	−2.79	−2.45	−2.89	29.1	31.8
s^0_{ex}/J K^{-1} mol^{-1}	−39.1	−40.1	−33.8	−39.2	25.5	35.3
h^0_{ex}/kJ mol^{-1}	−14.2	−14.7	−12.5	−14.6	36.7	42.3
$C_{P,ex}$/J K^{-1} mol^{-1}	45	48	34	43	−24	−32

[a] The parameters are obtaind by fitting the data to the second order expansion (eq 7).

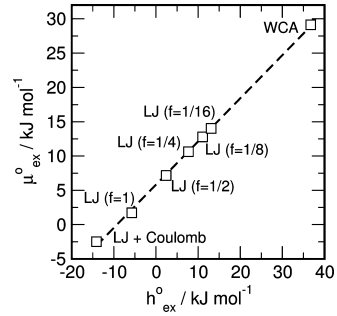

Figure 6. Correlation between the solvation free energy μ^0_{ex} and the solvation enthalpy h^0_{ex} dissolved in $[C_2mim][NTf_2]$ obtained for the different potential model variants of CO_2 at standard conditions. The dashed line represents a linear dependence with $\mu^0_{ex} = 0.63 h^0_{ex} + 5.83$ kJ mol^{-1}, inspired by Xie and Simha.[73]

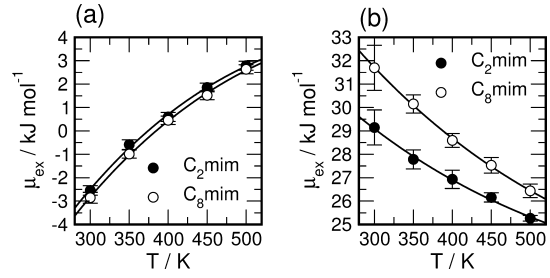

Figure 7. Temperature dependence of the excess chemical potential of CO_2 (a) and WCA-CO_2 (b) dissolved in $[C_2mim][NTf_2]$ and $[C_8mim][NTf_2]$.

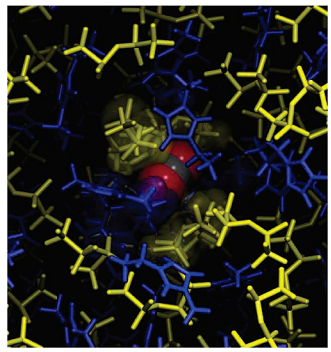

Figure 8. Snapshot showing the environment of a CO_2 molecule in [C_2mim][NTf_2], taken from the MD simulation. The surface of (heavy) solvent atoms found within a distance of less than 5 Å are shown as a semitransparent blob. Cations are shown in blue; anions are given in yellow.

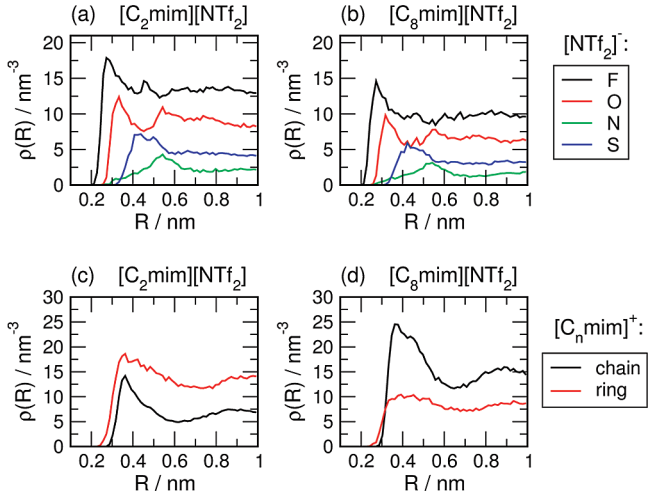

Figure 9. Proximal radial density distribution functions $\rho(R)$ of selected groups of solvent heavy atoms probed at a distance R from the CO_2 molecule at 350 K. (a, b) Density distributions of the atoms of the [NTf_2] anion in [C_2mim][NTf_2] (a) and [C_8mim][NTf_2] (b). (c, d) Density distributions of the heavy atoms of the cations. We distinguish two groups of atoms: the five atoms forming the imidazolium "ring" as well as the carbon atoms found in the alkane "chains" attached to the ring.

more likely to be the consequence of counter-compensating effects that almost cancel out. To give a qualitative impression, we have depicted the immediate environment of a CO_2 molecule dissolved in [C_2mim][NTf_2] in Figure 8.

To elucidate structural changes in the local environment of a dissolved carbon dioxide molecule in a quantitative fashion, however, we inspect the atom site density around CO_2. We use a procedure of calculating CO_2−IL "proximal radial density distribution functions" $\rho_{prox}(R)$, similar to Ashbaugh and Paulaitis[84,85] and also suggested earlier.[86,87] This representation is superior to atom−atom pair correlation functions for the purpose of this paper, since artifacts such as density depletion effects due to neighboring solute atoms are avoided. As reference sites, we take the positions of all three atoms within CO_2. The normalization volume s dR is defined by volume elements with a shortest distance R to any atom of CO_2. The nonspherical normalization volumes are computed numerically from a Monte Carlo procedure.

Figure 9 shows proximal radial density distribution functions calculated for selected sets of solvent atoms, grouped in anion and cation atoms, and obtained for [C_2mim][NTf_2] and [C_8mim][NTf_2], respectively. Atoms of the cations, given in

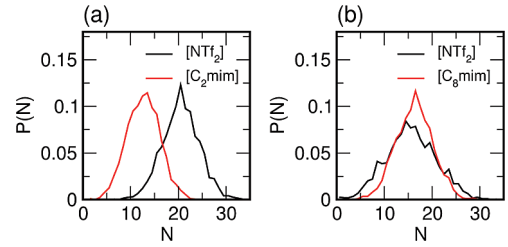

Figure 10. Distribution of the number of heavy (non-hydrogen) atoms of the anions and cations found within a distance of less than 5 Å to any atom of the carbon dioxide molecule at 350K. (a) [C_2mim][NTf_2]. (b) [C_8mim][NTf_2].

Figure 9, are separated into "ring" and "chain" atoms. Increasing the length of the alkane chain in [$C_n$mim] significantly shifts the weight of direct CO_2 contacts from ring atoms to chain atoms. An implication might be that adding functional groups to the alkyl chain to increase the IL−CO_2 interaction could be significantly more efficient for cations with longer alkane chains. Anion contacts are dominated by fluorine and oxygen atoms, whereas the CO_2 avoids direct contact with the nitrogen atom. The decreasing density of anion atoms around the CO_2 with increasing chain length indicates a shift toward more CO_2−cation contacts.

This is further substantiated by the distribution functions shown in Figure 10. Here, we draw the distribution functions of heavy-atom contacts of CO_2 with anion and cation sites. The distributions shown in Figure 10a clearly indicate that for [C_2mim][NTf_2], the interactions of the anion with CO_2 dominate. This is in line with the experimental observation that the [NTf_2] ion is important for high solubility of carbon dioxide, as pointed out by Cadena et al.[9] The highlighted "contacts" in the snapshot shown in Figure 8 illustrate this dominance of close CO_2−[NTf_2] interactions in [C_2mim][NTf_2]. With increasing chain length, however, the cation contacts increasingly compete with the anion contacts, as shown by the shift in the anion/cation contact distributions shown in Figure 10. The distribution suggests a significant difference of the structure and composition of the CO_2 solvation shell of the two ILs. Our results imply that the anion should play a stronger role in CO_2 solubility for Ils with shorter alkyl chains than for cations with longer alkyl chains. Reinspecting the experimental data, we found evidence that this is, indeed, the case. Bara et al.[23] report in a recent compilation of experimental data a CO_2 solubility increase of 116% for [C_2mim][NTf_2] vs [C_2mim][BF_4], whereas the solubility increase drops to 70% for [C_4mim][NTf_2] vs [C_4mim][BF_4]. Hence, we would like to emphasize that the apparent chain length insensitivity of the free energy of solvation might not necessarily lead us to the conclusion that the cation plays a minor role in the solvation process. Instead, our simulations suggest the possibility of an alternative scenario: The enhanced tendency of exclusion from the solvent, driven by an increasing cohesive interaction of the ILs, is counterbalanced by an increasing attractive van der Waals interaction with the cation.

4. Conclusion

The solubility of carbon dioxide in the ionic liquids of type 1-alkyl-3-methylimidazolium bis(trifluoromethylsulfonyl)imide ([$C_n$mim][NTf_2]) with varying chain lengths $n = 2, 4, 6, 8$ has been computed from molecular dynamics simulations, applying Bennett's overlapping distribution method, as well as Widom's particle insertion technique. By employing sufficiently high sampling rates, the results obtained from both techniques are found to agree with the error bars. In addition, we find excellent

agreement with available experimental data over a large temperature range from 300 to 500 K. Particularly, the solubility dependence on the alkyl chain length of the imidazolium cation is reproduced well. We find that the solvation free energy of carbon dioxide is remarkably insensitive to the alkane chain length, emphasizing the importance for using models providing accurate volumetric properties. The simulations reveal the experimentally observed "anomalous" temperature dependence of the CO_2, caused by a negative entropy of solvation. By systematically varying the interaction strength of CO_2, we show that the negative solvation entropy of CO_2 is not due to cavity effects, but caused by attractive solute−solvent interactions. The contribution of the van der Waals interactions is found to dominate. Comparing models with varying solute−solvent interaction strength, we find that the solvation free energy scales linearly with the solvation enthalpy, as previously suggested for polymers. The exact slope is likely to depend on the solvent and the nature of this relation needs to be further explored. The apparent chain length insensitivity of the solvation free energy of CO_2 is likely to be caused by counter-compensating effects, as the analysis of the composition of the solvation shell indicates significant changes.

Acknowledgment. This work has been supported by the German Science Foundation (DFG) priority program SPP 1191 with additional support from SFB 652. D.P. acknowledges support by the Rensselaer Polytechnic Institute.

References and Notes

(1) Wasserscheid, P.; Welton, T. *Ionic Liquids in Synthesis*, 2nd ed.; VCH-Wiley: Weinheim, 2008.
(2) Endres, F.; El Abedin, S. Z. *Phys. Chem. Chem. Phys.* **2006**, *8*, 2101–2116.
(3) Rogers, R. D.; Seddon, K. R. *Science* **2003**, *302*, 792–793.
(4) Lopes, J. N. A. C.; Padua, A. A. H. *J. Phys. Chem. B* **2006**, *110*, 3330–3335.
(5) Padua, A. A. H.; Gomes, M. F.; Lopes, J. N. A. C. *Acc. Chem. Res.* **2007**, *40*, 1087–1096.
(6) Köddermann, T.; Wertz, C.; Heintz, A.; Ludwig, R. *ChemPhysChem* **2006**, *7*, 1944–1949.
(7) Rebelo, L. P. N.; Lopes, J. N. C.; Esperanca, J. M. S. S.; Lachwa, H. J. R. G. J.; Najdanovic-Visak, V.; Visak, Z. P. *Acc. Chem. Res.* **2007**, *40*, 1114–1121.
(8) Anthony, J. L.; Maginn, E. J.; Brennecke, J. F. *J. Phys. Chem. B* **2002**, *106*, 7315–7320.
(9) Cadena, C.; Anthony, J. L.; Shah, J. K.; Morrow, T. I.; Brennecke, J. F.; Maginn, E. J. *J. Am. Chem. Soc.* **2004**, *126*, 5300–5308.
(10) Camper, D.; Scovazzo, P.; Koval, C.; Noble, R. *Ind. Eng. Chem. Res.* **2004**, *43*, 3049–3054.
(11) Camper, D.; Becker, C.; Koval, C.; Noble, R. *Ind. Eng. Chem. Res.* **2005**, *44*, 1928–1933.
(12) Camper, D.; Becker, C.; Koval, C.; Noble, R. *Ind. Eng. Chem. Res.* **2006**, *45*, 445–450.
(13) Finotello, A.; Bara, J. E.; Camper, D.; Noble, R. D. *Ind. Eng. Chem. Res.* **2008**, *47*, 3453–3459.
(14) Baltus, R. E.; Culbertson, B. H.; Dai, S.; Luo, H.; DePaoli, D. W. *J. Phys. Chem. B* **2004**, *108*, 721–727.
(15) Lee, B.; Outcalt, S. L. *J. Chem. Eng. Data* **2006**, *51*, 892–897.
(16) Kamps, A. P. S.; Tuma, D.; Xia, J. Z.; Maurer, G. *J. Chem. Eng. Data* **2003**, *48*, 746–749.
(17) Anthony, J. L.; Anderson, J. L.; Maginn, E. J.; Brennecke, J. F. *J. Phys. Chem. B* **2005**, *109*, 6366–6374.
(18) Kumelan, J.; Kamps, A. P. S.; Tuma, D.; Maurer, G. *J. Chem. Thermodyn.* **2006**, *38*, 1396–1401.
(19) Gomes, M. F. C. *J. Chem. Eng. Data* **2007**, *52*, 472–475.
(20) Muldoon, M. J.; Aki, S. N. V. K.; Anderson, J. L.; Dixon, J.; Brennecke, J. F. *J. Phys. Chem. B* **2007**, *111*, 9001–9009.
(21) Jacquemin, J.; Husson, P.; MajerDai, V.; Gomes, M. F. C. *J. Solution Chem.* **2007**, *36*, 967–979.
(22) Shi, W.; Maginn, E. J. *J. Phys. Chem. B* **2008**, *112*, 2045–2055.
(23) Bara, J. E.; Carlisle, T. K.; Gabriel, C. J.; Camper, D.; Finotello, A.; Gin, D. L.; Noble, R. D. *Ind. Eng. Chem. Res.* **2009**, *48*, 2739–2751.
(24) Blanchard, L. A.; Brennecke, J. F. *Ind. Eng. Chem. Res.* **2001**, *40*, 287–292.
(25) Blanchard, L. A.; Gu, Z. Y.; Brennecke, J. F. *J. Phys. Chem. B* **2001**, *105*, 2437–2444.
(26) Blanchard, L. A.; Hancu, D.; Beckman, E. J.; Brennecke, J. F. *Nature* **1999**, *399*, 28–29.
(27) Hert, D. G.; Anderson, J. L.; Aki, S. N. K.; Brennecke, J. F. *Chem. Commun.* **2005**, 2603–2605.
(28) Hanke, C. G.; Price, S. L.; Lynden-Bell, R. M. *Mol. Phys.* **2001**, *99*, 801–809.
(29) Morrow, T.; Maginn, E. J. *J. Phys. Chem. B* **2002**, *106*, 12807–12813.
(30) Margulis, C.; Stern, H.; Berne, B. *J. Phys. Chem. B* **2002**, *106*, 12017–12021.
(31) Wu, X. P.; Liu, Z. P.; Huang, S. P.; Wang, W. C. *Phys. Chem. Chem. Phys.* **2006**, *8*, 1096–1104.
(32) Lopes, J.; Deschamps, J.; Padua, A. *J. Phys. Chem. B* **2004**, *108*, 2038–20047.
(33) Köddermann, T.; Paschek, D.; Ludwig, R. *ChemPhysChem* **2007**, *8*, 2464–2470.
(34) Köddermann, T.; Paschek, D.; Ludwig, R. *ChemPhysChem* **2008**, *9*, 549–555.
(35) Paschek, D.; Köddermann, T.; Ludwig, R. *Phys. Rev. Lett.* **2008**, *100*, 115901.
(36) Pratt, L. R. *Annu. Rev. Phys. Chem.* **2003**, *53*, 409–436.
(37) Southall, N. T.; Dill, K. A.; Haymet, A. D. J. *J. Phys. Chem. B* **2002**, *106*, 521–533.
(38) Widom, B.; Bhimalapuram, P.; Koga, K. *Phys. Chem. Chem. Phys.* **2003**, *5*, 3085–3093.
(39) Chandler, D. *Nature (London)* **2005**, *437*, 640–647.
(40) Lynden-Bell, R. M.; Atamas, N. A.; Vasilyuk, A.; Hanke, C. G. *Mol. Phys.* **2002**, *100*, 3225–3229.
(41) Hanke, C. G.; Johansson, A.; Harper, J. B.; Lynden-Bell, R. M. *Chem. Phys. Lett.* **2003**, *374*, 85–89.
(42) Deschamps, J.; Gomes, M. F. C.; Padua, A. A. H. *ChemPhysChem* **2004**, *5*, 1049–1052.
(43) Shah, J. K.; Maginn, E. J. *Fluid Phase Equilib.* **2004**, *195*, 222–223.
(44) Shah, J. K.; Maginn, E. J. *J. Phys. Chem. B* **2005**, *109*, 10395–10405.
(45) Kumelan, J.; Kamps, A. P. S.; Urukova, I.; Tuma, D.; Maurer, G. *J. Chem. Thermodynamics* **2005**, *37*, 595–602.
(46) Urukova, I.; Vorholz, J.; Maurer, G. *J. Phys. Chem. B* **2005**, *109*, 12154–12159.
(47) Kumelan, J.; Kamps, A. P. S.; Tuma, D.; Maurer, G. *Ind. Eng. Chem. Res.* **2007**, *46*, 8236–8240.
(48) Shi, W.; Maginn, E. J. *J. Chem. Theory Comput.* **2007**, *3*, 1451–1463.
(49) Andersen, H. C.; Weeks, J. D.; Chandler, D. *Phys. Rev. A* **1971**, *4*, 1597–1607.
(50) Harris, J. G.; Yung, K. H. *J. Phys. Chem.* **1995**, *99*, 12021–12024.
(51) Ciccotti, G.; Ferrario, M.; Ryckaert, J. *Mol. Phys.* **1982**, *47*, 1253–1264.
(52) Vargaftik, N. B. Tables on the Thermophysical Properties of Liquids and Gases. In *Normal and Dissociated States*, 2nd ed.; Hemisphere Publishing Corporation: Washington, London, 1975.
(53) Etesse, P.; Zega, J. A.; Kobayashi, R. *J. Chem. Phys.* **1992**, *97*, 2022–2029.
(54) Lindahl, E.; Hess, B.; van der Spoel, D. *J. Mol. Model.* **2001**, *7*, 306–317.
(55) Paschek, D. *MOSCITO 4: MD simulation package*, 2008; http://ganter.chemie.tu-dortmund.de/MOSCITO.
(56) Nosé, S. *Mol. Phys.* **1984**, *52*, 255–268.
(57) Hoover, W. G. *Phys. Rev. A* **1985**, *31*, 1695–1697.
(58) Parrinello, M.; Rahman, A. *J. Appl. Phys.* **1981**, *52*, 7182–7180.
(59) Nosé, S.; Klein, M. L. *Mol. Phys.* **1983**, *50*, 1055–1076.
(60) Essmann, U.; Perera, L.; Berkowitz, M. L.; Darden, T. A.; Lee, H.; Pedersen, L. G. *J. Chem. Phys.* **1995**, *103*, 8577–8593.
(61) Ryckaert, J. P.; Ciccotti, G.; Berendsen, H. J. C. *J. Comp. Phys.* **1977**, *23*, 327–341.
(62) Tariq, M.; Forte, P. A. S.; Costa Gomes, M. F.; Canongia Lopes, J. N.; Rebelo, L. P. N. *J. Chem. Thermodyn.* **2009**, *41*, 790–798.
(63) Flyvbjerg, H.; Petersen, H. G. *J. Chem. Phys.* **1989**, *91*, 461–466.
(64) Kennan, R. P.; Pollack, G. L. *J. Chem. Phys.* **1990**, *93*, 2724–2735.
(65) Widom, B. *J. Chem. Phys.* **1963**, *39*, 2808–2812.
(66) Beck, T. L.; Paulaitis, M. E.; Pratt, L. R. *The Potential Distribution Theorem and Models of Molecular Solutions*; Cambridge University Press: Cambrigde, UK, 2006.
(67) Bennett, C. H. *J. Comput. Phys.* **1976**, *22*, 245–268.
(68) Shing, K. S.; Gubbins, K. E. *Mol. Phys.* **1983**, *49*, 1121–1138.
(69) Frenkel, D.; Smit, B. *Understanding Molecular Simulation. From Algorithms to Applications*, 2nd ed.; Academic Press: San Diego, 2002.
(70) Paschek, D. *J. Chem. Phys.* **2004**, *120*, 6674–6690.
(71) Roberts, J. E.; Schnitker, J. *J. Chem. Phys.* **1994**, *101*, 5024–5031.

(72) Paschek, D. *J. Chem. Phys.* **2004**, *120*, 10605–10617.
(73) Xie, H.; Simha, R. *Polym. Int.* **1997**, *44*, 348–355.
(74) Marsh, K. N.; Brennecke, J. F.; Chirico, R. D.; Frenkel, M.; Heintz, A.; Magee, J. W.; Peters, C. J.; Rebelo, L. P. N.; Seddon, K. R. *Pure Appl. Chem.* **2009**, *81*, 781–790.
(75) Chirico, R. D.; Diky, V.; Magee, J. W.; Frenkel, M.; Marsh, K. N. *Pure Appl. Chem.* **2009**, *81*, 791–828.
(76) Van Krevelen, D. W.; Hoftyzer, P. J. *Properties of Polymers: Their Esitmation and Correlationwith Chemical Structure*, 2nd ed.; Elsevier: Amsterdam, 1967.
(77) Sato, Y.; Takikawa, T.; Takishima, S.; Masuoka, H. *J. Supercrit. Fluids* **2001**, *19*, 187–198.
(78) Wilhelm, E.; Battino, R. *Chem. Rev.* **1973**, *73*, 1–9.
(79) Sanchez, I. C.; Lacombe, R. H. *Macromolecules* **1978**, *11*, 1145–1156.
(80) Simha, R.; Somcynsky, T. *Macromolecules* **1969**, *2*, 342–350.
(81) Hummer, G.; Garde, S.; García, A. E.; Pratt, L. R. *Chem. Phys.* **2000**, *258*, 349–370.
(82) Kollman, P. A. *Chem. Rev.* **1993**, *93*, 2395–2417.
(83) Scovazzo, P.; Camper, D.; Kieft, J.; Posthusta, J.; Koval, C.; Noble, R. *Ind. Eng. Chem. Res.* **2004**, *43*, 6855–6860.
(84) Ashbaugh, H. S.; Paulaitis, M. E. *J. Phys. Chem.* **1996**, *100*, 1900–1913.
(85) Ashbaugh, H. S.; Paulaitis, M. E. *J. Am. Chem. Soc.* **2001**, *123*, 10721–10728.
(86) Mehrotra, P. K.; Beveridge, D. L. *J. Am. Chem. Soc.* **1980**, *102*, 4287–4294.
(87) Levitt, M.; Sharon, R. *Proc. Natl. Acad. Sci. USA* **1988**, *85*, 7557–7561.

JP9055285